Heliyon

ELSEVIER

Received:
8 June 2016
Revised:
23 September 2016
Accepted:
24 October 2016

Heliyon 2 (2016) e00190

Influence of atomic bonds on the properties of the laxative drug sodium picosulphate

Davide Romani [a], **Isabel Salas Tonello** [b], **Silvia Antonia Brandán** [b,*]

[a] *SST, Servicio sanitario della Toscana, Azienda USL 9 di Grosseto, Via Cimabue, 109, 58100 Grosseto, Italy*

[b] *Cátedra de Química General, Instituto de Química Inorgánica, Facultad de Bioquímica, Química y Farmacia, Universidad Nacional de Tucumán, Ayacucho 471,(4000), San Miguel de Tucumán, Tucumán, Argentina*

* Corresponding author.

E-mail address: sbrandan@fbqf.unt.edu.ar (S.A. Brandán).

Abstract

In this work, the influence of the different S═O, S−O, N···H, O···H, Na···O bonds present in the structures of the powerful laxative drug, sodium picosulphate in gas and aqueous solution phases were studied combining the density functional theory (DFT) calculations with the experimental available infrared, ^{1}H NMR and UV-visible spectra. The structural, topological, electronic and vibrational properties were investigated in both media by using the hybrid B3LYP/6-31G* method and the integral equation formalism variant polarised continuum model (IEFPCM). Here, the characteristics of the S═O, S−O, N···H, O···H, Na···O bonds were completely revealed by using atomic charges, natural bond orbital (NBO) and atoms in molecules (AIM) studies. The infrared, ^{1}H NMR, ^{13}C NMR and UV-visible spectra are in reasonable concordance with those experimental available in the literature. The vibrational analysis of sodium picosulphate was performed considering C_{3V} symmetries for both SO_4^{2-} groups and the complete assignments of the 126 vibration modes were reported in gas phase and aqueous solution together with their corresponding force fields. In addition, the reactivities of sodium picosulfate increase in solution due to their ionic characteristic which probably justifies their behaviour as a stimulant cathartic and their easy metabolic conversion, as reported in the literature.

Keywords: Pharmaceutical science, Theoretical chemistry, Inorganic chemistry

http://dx.doi.org/10.1016/j.heliyon.2016.e00190

1. Introduction

The sodium salts containing SO_4^{2-} or SO_3^{2-} groups in their structures are employed as reactive in numerous and important industries, as was reported by Periasamy et al. [1]. Structurally, two modes of coordination in particular, monodentate or bidentate, are expected for these groups in different compounds [2, 3, 4]. Normally, those sodium salts when are linked to different organic rings present interesting biological activities which due to their ionic characteristic are highly used in the pharmaceutical industry to facilitate the incorporation of drugs to the human organism or as an intermediate in the preparation of other drugs [4]. For these reasons, the structures and properties of pharmaceutical drugs containing those salts are of great interest to their identifications by using different spectroscopic techniques, such as the vibrational spectroscopy and also, to know and predict their reactivities and behaviours in the different media in which they are present. The aim of this work is to study the structural and vibrational properties of anhydrous sodium picosulphate or picosulfate, a stimulant laxative drug orally administered to patients in preparations for colonoscopy [5, 6, 7, 8], taking into account that, so far, these properties were not reported. Actually, the control and the quantitative analysis of this drug are performed by using the high performance liquid chromatographic (HPLC) because this technique is one of the most studied [9, 10]. The chemical name of this compound is the 4,4′-(2-pyridinylmethylene) bisphenol bis (hydrogen sulfate) (ester) disodium salt. This salt itself is pharmacologically inactive but it is converted by bacterial hydrolase in the human organism to the pharmacologically active metabolite, bis(*p*-hydroxyphenyl)-2-pyridylmethane [6]. Here, we have reported a detailed study on the structural and vibrational properties of sodium picosulfate combining the DFT calculations with the experimental available FTIR, NMR and UV-visible spectra in gas phase and in aqueous solution taking into account that this salt is soluble in water. The initial structures of this salt in these two media were optimized by using the hybrid B3LYP/6-31G* level of theory [11, 12]. After that, NBO [13, 14] and AIM [15, 16] calculations were performed in order to investigate the characteristics of the different pyridinyl and phenyl rings and of the Na−O, S═O and S−O bonds together with their topological properties. The force fields for the compound in the two media were computed by using a generalized valence force field (GVFF) [17, 18] and the normal modes calculations with the Molvib program [19]. Then, the complete assignments of the 126 vibration normal modes predictable for sodium picosulfate were reported in both media using the potential energy distribution (PED). In this paper, the structural, topological and vibrational properties for sodium picosulfate together with their vibrational assignment are reported for the first time. This way, the sodium picosulfate salt could be easily identified in different media by means of the vibrational spectroscopy.

http://dx.doi.org/10.1016/j.heliyon.2016.e00190

2. Methodology

The initial anhydrous sodium picosulfate (APS) structure was modelled by using the *GaussView* program [20] taking into account a C_{3v} symmetry for the two sulfate groups, in accordance with the experimental structure observed for the potassium borosulfate [2]. After that, the Cartesian coordinates were optimized in gas and aqueous solution phases using the hybrid B3LYP/6-31G* method [11, 12] with the Gaussian 09 program [21]. The influence of the solvent on their properties were studied by using the self-consistent reaction field (SCRF) method together with the IEFPCM model at the same level of theory [22, 23]. The volume variation that experiment the salt in water was also computed using the Moldraw program [24] whiles the solvation energy involved in this process was calculated using the solvation model [25]. Both stable structures represent minima in the potential energy surface because all the frequencies are positive. Fig. 1 show the optimized structure of sodium picosulfate together with the numbering of the atoms while the detailed identification of the pyridinyl and phenyl rings is presented in Fig. 2. The characteristics of the three rings and of the Na−O, S═O and S−O bonds were investigated by using the atomic charges, bond orders, molecular electrostatic potentials (MEP) surface, stabilization energies, topological properties which were computed in both media with the NBO 3.1 and AIM2000 programs [14, 16]. Here, the MEP surface of the salt in the gas phase was built with the aid of the *GaussView* program [20] while the corresponding values were obtained using the

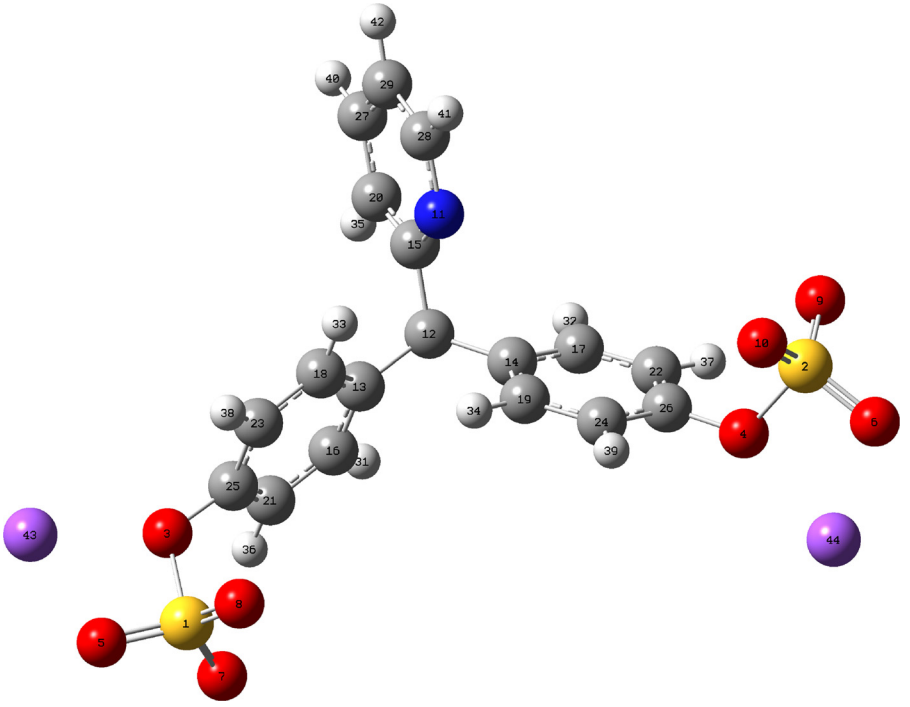

Fig. 1. Theoretical molecular structure of anhydrous sodium picosulfate and the atoms labelling.

http://dx.doi.org/10.1016/j.heliyon.2016.e00190

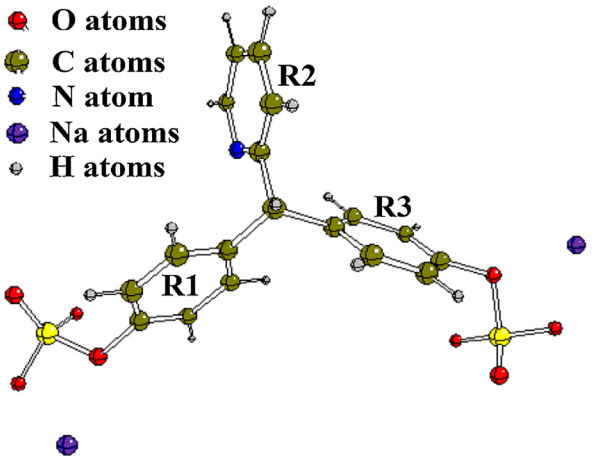

Fig. 2. Detailed structure of anhydrous sodium picosulfate showing the pyridinyl and phenyl rings.

Merz-Kollman (MK) charges [26]. Additionally, the frontier molecular orbitals and some descriptors were calculated in order to predict the reactivity and behaviours in the two media studied [27, 28, 29, 30, 31, 32, 33]. On the other hand, the Molvib program [19] was used to transform the force fields initially expressed in Cartesian coordinates to natural internal coordinates. After that, the Potential Energy Distribution (PED) were computed from the scaled quantum mechanics (SQM) force fields in both media using the same level of theory in order to perform the complete assignments considering the PED contributions $\geq 10\%$. The ^{1}H-NMR and ^{13}C-NMR spectra in aqueous solution were predicted by using the GIAO method [34] while the time dependent density functional theory (TD-DFT) calculations were employed to predict the electronic spectra in solution at the same level of theory.

3. Results and discussion

3.1. Geometrical parameters in both media

The calculated total energies, dipole moments, volume variation and solvation energy for APS in gas and aqueous solution phases can be seen in Table 1. The results show a notable increase in the dipole moment value from 11.06 D in gas phase to 15.14 D in solution while the volume in solution increase from 471.2 Å^3 in gas phase to 484.5 Å^3 in solution showing a volume variation of 13.3 Å^3. Fig. 3 shows that in solution an additional change in the direction of the dipole moment is observed due to the separation between the pairs of SO_4^{2-} and Na^+ ions. As was above mentioned the volumes in both media were calculated with the Moldraw program [24] using the B3LYP/6-31G* method. Thus, the expansion of the volume observed in solution is attributed to the calculated high corrected solvation energy value (-254.38 kJ/mol) as a consequence of the hydration of this salt with the water

http://dx.doi.org/10.1016/j.heliyon.2016.e00190

Table 1. Calculated total (E) and relative energies (ΔE), dipole moments, volume variation and solvation energy for anhydrous sodium picosulphate in gas and aqueous solution phases.

B3LYP/6-31G*		
GAS		
E (hartree)	μ (D)	V (Å^3)
−2471.27	11,06	471,2
PCM		
E (hartree)	μ (D)	V (Å^3)
−2471.36	15,14	484,5
Solvation energy		
$\Delta G_u^{\#}$	ΔG_{ne}	ΔG_c
−236.07	18,31	−254,38
ΔV (Å^3)=13.3		

molecules. Note that the corrected solvation energy has higher value than the corresponding uncorrected because the total non electrostatic terms due to the cavitation, dispersion and repulsion energies, computed with the IEFPCM [22, 23] and SM [25] models were added.

So far, the crystalline and molecular structure of APS were not experimentally determined and, for this reason, the calculated geometrical parameters for the three rings of APS in both media were compared with those experimental values observed by Sun et al. [35] for Bis[μ−1,2-diphenyl-*N*,*N*′-bis-(di-2-pyridyl-methyl-eneamino)ethane-1,2-diimine]disilver(I) bis-(hexa-fluorido-phosphate) acetonitrile disolvate because it compound have similar pyridyl and phenyl rings in their structure. On the other hand, the calculated parameters for the SO_4^{2-} groups were compared with those experimental recently reported for a new sulfate salt, sodium magnesium sulfate deca-hydrate, $Na_2Mg(SO_4)_2.10\ H_2O$ by Leduc et al. [36] because it compound present two sulfate groups linked to sodium atoms, such as APS. These comparisons were performed by means of the root-mean-square deviation (RMSD) values which are summarized in Table 2 together with the geometrical parameters for APS in both media. Regarding the results we clearly observed that in general the calculations in gas phase predicted higher values for the bond lengths and angles related to the pyridyl and phenyl rings than for the SO_4^{2-} groups while in solution are most notable the increase in the bond lengths

http://dx.doi.org/10.1016/j.heliyon.2016.e00190

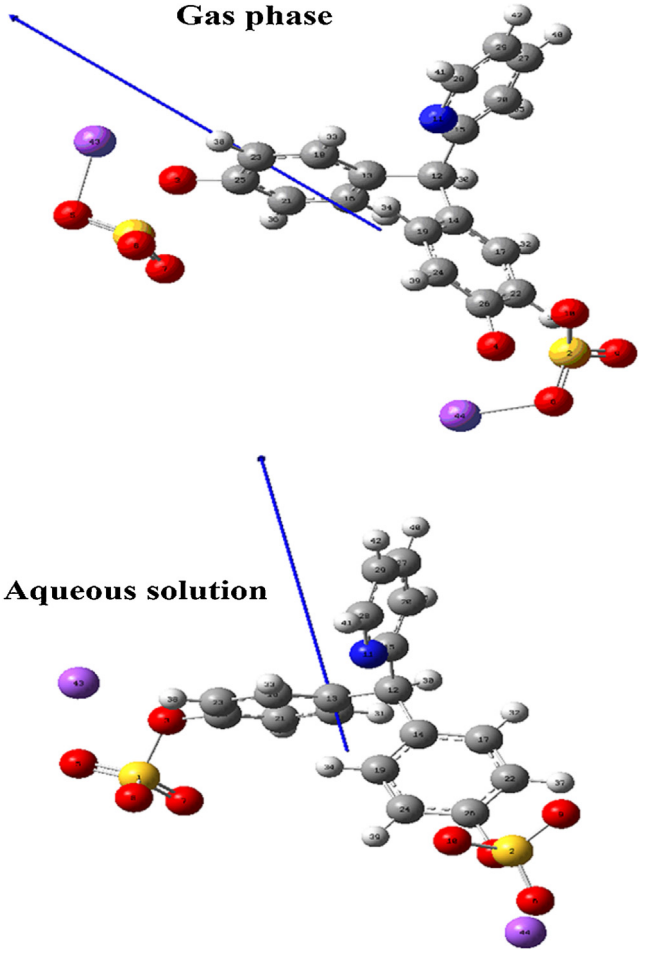

Fig. 3. Dipole moment directions for the anhydrous sodium picosulfate salt in gas phase (top) and in aqueous solution (bottom) showing the corresponding magnitudes and orientations of their vectors.

corresponding to the SO_4^{2-} groups, as expected due to the affinity of these groups with the water. The exhaustive analysis show that from the four S−O bonds in the sulphate groups three S═O bonds present lower and similar values, showing clearly their double bond character, while the remain S1−O3 and S2−O4 distances have higher values, confirming this way, the C_{3v} symmetry considered for these groups. In solution, important changes in the S═O and S−O distances are observed, thus, whereas two S−O bonds are enlarged the other two are shortened, as shown Table 2. Other very important observation is the remarkable increase in solution of both O-Na distances evidencing the ionic characteristics of these bonds, as expected due to the presence of two SO_4^{2-} groups and two Na^+ cations in the structure of APS.

http://dx.doi.org/10.1016/j.heliyon.2016.e00190

Table 2. Comparison of calculated geometrical parameters for the anhydrous with the corresponding experimental ones.

B3LYP/6-31G*[a]			Experimental	
Parameter	**Gas**	**PCM**	**Exp[b]**	**Exp[c]**
		Bond lengths (Å)		
C25-O3	1.388	1.401		
C26-O4	1.387	1.402		
C12-C13	1.534	1.530		
C12-C14	1.532	1.531		
C12-C15	1.528	1.530		
C13-C16	1.402	1.402	1.372	
C16-C21	1.392	1.394	1.361	
C21-C25	1.396	1.393	1.369	
C25-C23	1.394	1.392	1.361	
C23-C18	1.395	1.395	1.371	
C18-C13	1.401	1.402	1.375	
C14-C17	1.400	1.403	1.372	
C17-C22	1.394	1.394	1.361	
C22-C26	1.394	1.393	1.369	
C26-C24	1.396	1.392	1.361	
C24-C19	1.392	1.395	1.371	
C19-C14	1.401	1.400	1.375	
C15-N11	1.342	1.344	1.347	
N11-C28	1.337	1.343	1.324	
C28-C29	1.394	1.392	1.381	
C29-C27	1.393	1.394	1.369	
C27-C20	1.393	1.392	1.365	
C20-C15	1.401	1.401	1.361	
O5-Na43	2.151	2.263		2.518
O6-Na44	2.156	2.263		2.518
S1-O3	1.810	1.720		1.488
S1-O5	1.500	1.493		1.481
S1-O7	1.461	1.472		1.463
S1-O8	1.460	1.472		1.477
S2-O4	1.807	1.719		1.488
S2-O6	1.500	1.493		1.481
S2-O9	1.461	1.472		1.463
S2-O10	1.459	1.472		1.477

(*Continued*)

http://dx.doi.org/10.1016/j.heliyon.2016.e00190

Table 2. (*Continued*)

B3LYP/6-31G*,[a]			Experimental	
Parameter	**Gas**	**PCM**	**Exp[b]**	**Exp[c]**
RMSD	**0.132**	**0.095**		
		Dihedral angles (°)		
C12-C13-C16	118.4	118.9	120.9	
C12-C13-C18	123.3	122.5	121.3	
C12-C14-C17	119.5	118.3	120.9	
C12-C14-C19	122.0	123.1	121.3	
C12-C15-N11	118.1	118.4		
C12-C15-C20	120.1	119.3		
O7=S1=O8	118.7	115.6		109.6
O7=S1=O5	114.9	114.7		109.6
O8=S1=O5	115.3	115.0		109.3
O3-S1=O8	94.9	105.7		108.9
O9=S2=O10	118.6	115.6		109.6
O9=S2=O6	114.8	114.8		109.6
O6=S2=O10	115.3	114.9		109.3
O4-S2=O6	94.7	96.9		108.9
S1-O5-Na43	103.8	104.4		87.4
S2-O6-Na44	103.9	104.3		87.4
RMSD	**9.4**	**8.2**		
		Dihedral angles (°)		
C15-C12-C13-C18	−39.3	−41.3		
C15-C12-C14-C19	72.2	96.0		
C14-C12-C15-C20	119.8	139.4		
C14-C12-C15-N11	−59.2	−41.2		
C25-O3-S1=O5	177.2	172.6		
O3-S1=O5-Na43	0.0	−2.6		−20.0
C26-O4-S2=O6	176.7	178.4		
O4-S2=O6-Na44	−0.4	−0.7		−20.0
RMSD	**19.8**	**18.4**		

[a] This work.
[b] [35].
[c] [36].

http://dx.doi.org/10.1016/j.heliyon.2016.e00190

3.2. NPA charges, bond orders and MEP surface studies

The ionic nature of APS is clearly evidenced by the geometrical parameters principally due to the two SO_4^{2-} groups and the two Na^+ cations which suggest the importance to study the charge distributions on their structures in both media and, besides the nature of the different bonds. For these reasons, we have studied two charge's types which are the natural population atomic (NPA) and the MK charges [26], the bond orders expressed by the Wiberg indexes and the molecular electrostatic potentials (MEPs). With the MK charges it is possible to calculate the MEP surface values in the two media while their surfaces mapped have permitted to observe the electrophilic and nucleophilic regions by their different colorations. All these properties are presented in Table 3. First, analyzing the charges we observed that both charges predicted higher positive values on the two S atoms than the two Na atoms but, in general, the values observed in the NPA charges are very different from those MK charges. For instance, the NPA charges on all the S, O and H atoms in both media are higher than the other ones while on the N atoms are observed lower NPA values. In relation to the charges on the C atoms with hybridizing sp^2, we observed negative signs on five C atoms belonging to the phenyl R1 and R2 rings, these are those rings linked to the SO_4^{2-} groups while in the pyridyl rings R3 only three C atoms have negative signs because the N atoms of these rings are also predicted by the calculations with negative signs. On the other hand, both charges predicted negative signs on the C12 atoms with hybridizing sp^3 in both media. Both charges reveal clearly the characteristics ionic of the two sulphate groups and the two Na atoms.

When the MEP surface values in both media are analyzed we observed a decreasing in the negative values according to the following order: S > Na > O > C > H where the MEP values on the O atoms linked to the rings, these are the C25-O3 and C26-O4 bonds, decreasing their values in solution while the remain O atoms belonging to the SO_4^{2-} groups exhibit increase in their corresponding MEP surface values. Obviously, the decrease and increase in the MEP surface values are strongly related to the MK charges, as observed in Table 3.

In relation to the bond orders, clearly Table 3 evidence the low bond order values observed in the two Na atoms being lower in solution, this way, the ionic behaviour of these atoms in both media is confirmed. In relation to the O atoms of both SO_4^{2-} groups we observed that the O5 and O6 atoms present the lower values because they are linked to the S and Na atoms and their values slightly decrease in solution by the same reason before explained. Regarding the values for the C atoms, we observed that those with hybridizing sp^2, the C13, C14 and C15 atoms, have the higher values while the C25 and C26 atoms which are linked to O atoms present the lower values, as expected due to the ionic characteristics of both SO_4^{2-} groups. The Wiberg bond index matrix in the NAO basis in gas phase shows bond order

http://dx.doi.org/10.1016/j.heliyon.2016.e00190

Table 3. Atomic MK and NPA charges, Molecular electrostatic potentials (MEP) and bond orders (Wiberg indexes) for anhydrous sodium picosulfate in both media at B3LYP/6-31G* level of theory.

Atoms	MK		NPA		MEP		Wiberg index	
	Gas	PCM	Gas	PCM	Gas	PCM	Gas	PCM
1S	1.137	1.141	2.537	2.564	−58.941	−58.949	4.210	4,217
2S	1.137	1.140	2.539	2.564	−58.948	−58.958	4.210	4,217
3 O	−0.759	−0.703	−0.847	−0.841	−22.284	−22.274	1.759	1,770
4 O	−0.752	−0.713	−0.846	−0.842	−22.291	−22.283	1.763	1,769
5 O	−0.661	−0.669	−1.055	−1.065	−22.332	−22.341	1.489	1,478
6 O	−0.662	−0.673	−1.055	−1.066	−22.339	−22.350	1.488	1,476
7 O	−0.484	−0.502	−0.925	−0.944	−22.345	−22.363	1.670	1,638
8 O	−0.479	−0.508	−0.918	−0.942	−22.345	−22.364	1.679	1,641
9 O	−0.489	−0.504	−0.926	−0.945	−22.352	−22.373	1.667	1,637
10 O	−0.476	−0.500	−0.917	−0.941	−22.353	−22.373	1.681	1,641
11N	−0.559	−0.579	−0.478	−0.459	−18.363	−18.367	3.074	3,073
12C	−0.215	−0.521	−0.291	−0.294	−14.721	−14.720	3.958	3,958
13C	−0.052	0.124	−0.026	−0.028	−14.733	−14.728	4.003	4,003
14C	0.179	0.296	−0.029	−0.024	−14.739	−14.737	4.004	4,005
15C	0.575	0.757	0.242	0.233	−14.696	−14.698	3.988	3,992
16C	−0.043	−0.122	−0.217	−0.215	−14.742	−14.736	3.947	3,947
17C	−0.233	−0.231	−0.220	−0.218	−14.746	−14.745	3.949	3,948
18C	−0.071	−0.202	−0.226	−0.227	−14.746	−14.739	3.934	3,936
19C	−0.105	−0.272	−0.205	−0.204	−14.751	−14.749	3.938	3,940
20C	−0.418	−0.520	−0.262	−0.265	−14.730	−14.731	3.944	3,944
21C	−0.380	−0.286	−0.255	−0.249	−14.744	−14.737	3.940	3,940
22C	−0.288	−0.209	−0.257	−0.250	−14.752	−14.747	3.939	3,943
23C	−0.336	−0.243	−0.253	−0.248	−14.742	−14.736	3.949	3,946
24C	−0.290	−0.210	−0.255	−0.245	−14.749	−14.748	3.949	3,944
25C	0.575	0.478	0.284	0.280	−14.686	−14.678	3.905	3,900
26C	0.505	0.430	0.290	0.279	−14.691	−14.689	3.905	3,900
27C	0.105	0.136	−0.193	−0.195	−14.719	−14.720	3.943	3,944
28C	0.297	0.288	0.034	0.032	−14.703	−14.706	3.927	3,927
29C	−0.367	−0.377	−0.279	−0.280	−14.729	−14.731	3.943	3,943
30H	0.064	0.127	0.252	0.256	−1.118	−1.114	0.939	0,937
31H	0.120	0.133	0.234	0.236	−1.111	−1.105	0.947	0,946
32H	0.146	0.136	0.231	0.232	−1.115	−1.113	0.948	0,948
33H	0.132	0.161	0.256	0.255	−1.118	−1.111	0.937	0,938
34H	0.126	0.201	0.252	0.249	−1.124	−1.123	0.938	0,940

(*Continued*)

http://dx.doi.org/10.1016/j.heliyon.2016.e00190

Table 3. (*Continued*)

Atoms	MK		NPA		MEP		Wiberg index	
	Gas	PCM	Gas	PCM	Gas	PCM	Gas	PCM
35H	0.163	0.184	0.240	0.238	−1.096	−1.096	0.944	0,945
36H	0.201	0.184	0.257	0.258	−1.110	−1.103	0.936	0,936
37H	0.199	0.164	0.260	0.253	−1.118	−1.112	0.935	0,938
38H	0.166	0.156	0.241	0.246	−1.106	−1.100	0.944	0,941
39H	0.159	0.165	0.240	0.252	−1.113	−1.114	0.945	0,939
40H	0.100	0.094	0.242	0.241	−1.092	−1.092	0.943	0,943
41H	0.053	0.065	0.224	0.228	−1.107	−1.111	0.951	0,950
42H	0.161	0.159	0.243	0.242	−1.095	−1.096	0.943	0,943
43 Na	0.908	0.910	0.919	0.925	−35.350	−35.329	0.165	0,151
44 Na	0.912	0.915	0.920	0.925	−35.358	−35.338	0.164	0,151

values of 0.460 for the S1−O3 and S2−O4 bonds indicating higher polarizations of these two bonds in relation to the other ones. This way, these bonds show different characteristics than the other ones, as will see later.

The study of the MEP surface mapped surfaces of APS in both media at the B3LYP/6-31G* level of theory show strong blue colorations on the two Na atoms

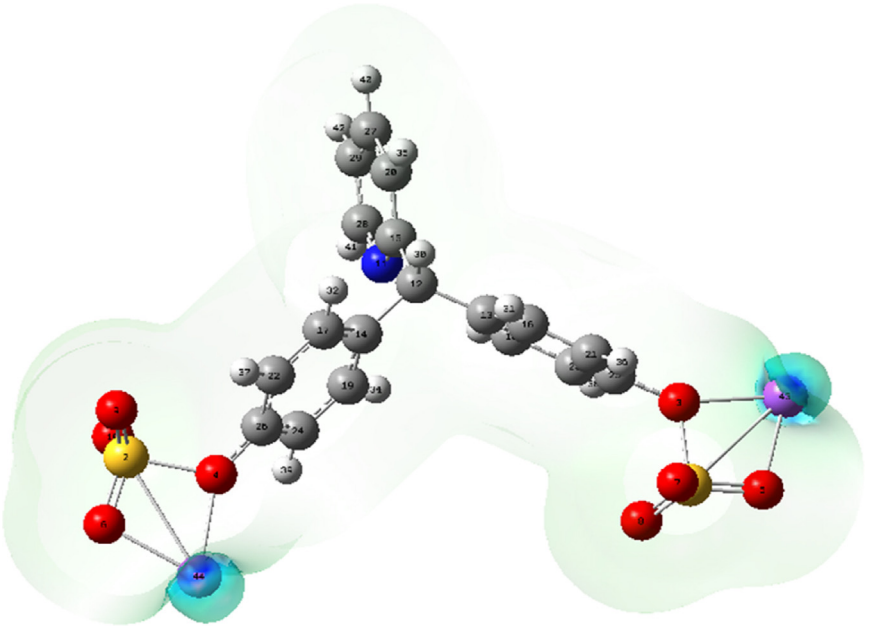

Fig. 4. Calculated electrostatic potential surfaces on the molecular surface of anhydrous sodium picosulfate in gas phase. Color ranges, in au: from red −1.186 to blue ++1.186. B3LYP functional and 6-31G* basis set. Isodensity value of 0.005.

http://dx.doi.org/10.1016/j.heliyon.2016.e00190

and green on remain atoms, this way, Fig. 4 support the nature electrophilic of this salt in both media. Note that the green colour indicated inert sites, as expected because they correspond to the three rings. Obviously, the blue colour on both Na atoms indicate probable sites reacting with potential biological nucleophiles. Evidently, the mapped surfaces could in part explain the laxative property observed for APS in solution.

3.3. NBO and AIM analysis

The above studies have showed the ionic characteristics of APS in both media but the study of the interactions between the involved SO_4^{2-} and Na^+ ions is also important in relation to their stabilities in both media. Hence, the stabilization energies and the topological parameters were calculated by using the NBO [14] and AIM [16] programs. Table 4 shows the main delocalization energy for APS in gas and in aqueous solution phases at B3LYP/6-31G* level of theory. Three important $\Delta E_{\pi \circledR \pi^*}$, $\Delta E_{n \rightarrow \sigma^*}$ and $\Delta E_{\pi^* \rightarrow \pi^*}$ charge transfers are observed in both media and other two $\Delta E_{\sigma \rightarrow \pi^*}$ and $\Delta E_{\sigma \rightarrow \sigma^*}$ charge transfers with lower values are also observed. The most important delocalization energy values are transitions from bonding orbitals C=C or C=N bonds to antibonding orbitals C=C, C=N or S=O bonds observed on the three rings and from the lone pairs of the O atoms of both SO_4^{2-} groups to antibonding orbitals S=O bonds. Notice that the two $\Delta E_{\sigma \rightarrow \pi^*}$ charge transfers are only observed in gas phase. Obviously, the total ΔE_{Total} contribution reveals the high stability of APS in both media, but specifically in solution, as expected due to their ionic characteristics.

The Bader's theory [15] is very interesting to explain the characteristics of inter and intra-molecular interactions in different compounds by using their topological properties which can be calculated with the AIM2000 program [16]. Thus, the electron density distribution, $\rho(r)$, the Laplacian values, $\nabla^2\rho(r)$, the eigenvalues $(\lambda 1, \lambda 2, \lambda 3)$ of the Hessian matrix and, the $|\lambda 1|/\lambda 3$ ratio calculated in the bond critical points (BCPs) reveal the interaction's types. Hence, the interaction is of hydrogen bonds or ionic interaction when $|\lambda 1|/\lambda 3 < 1$ and $\nabla^2\rho(r) > 0$ [37]. Here, these parameters for APS in both media at B3LYP/6-31G* level of theory are presented in Table 5. The values of those parameters in the BCPs show clear differences among the S−O bonds of both SO_4^{2-} groups in both media, as observed in Table 5. For instance, three S−O bonds of each SO_4^{2-} group show $\rho(r)$ values between 0.29 and 0.26 a.u. with $\nabla^2\rho(r) > 0$ and high values indicating that these interactions are highly polar covalent and are called closed-shell interactions while the S1−O3 and S2−O4 bonds present $\rho(r)$ values relatively high (0.3 and 0.1 a.u.) and negative of $\nabla^2\rho(r)$ values (-0.2 and -0.1 a.u.) demonstrating that these interactions are called shared interaction which are typical of covalent bonds. On the other hand, in gas phase are observed other eight closed-shell interactions ($\nabla 2\rho(r) > 0$) of which four are ionic with low $\rho(r)$ and high $\nabla^2\rho(r)$ (Na43···O3,

http://dx.doi.org/10.1016/j.heliyon.2016.e00190

Table 4. Main delocalization energy (in kJ/mol) for anhydrous picosulfate in gas and in aqueous solution phases at B3LYP/6-31G* level of theory.

Delocalization	Gas	PCM
$\pi N11\text{-}C15 \rightarrow \pi^*C20\text{-}C27$	53.80	55.26
$\pi N11\text{-}C15 \rightarrow \pi^*C28\text{-}C29$	115.16	112.15
$\pi C13\text{-}C18 \rightarrow \pi^*C16\text{-}C21$	85.10	84.52
$\pi C13\text{-}C18 \rightarrow \pi^*C23\text{-}C25$	88.91	90.04
$\pi C14\text{-}C17 \rightarrow \pi^*C19\text{-}C24$	83.77	
$\pi C14\text{-}C17 \rightarrow \pi^*C22\text{-}C26$	85.48	
$\pi C14\text{-}C19 \rightarrow \pi^*C17\text{-}C22$		86.65
$\pi C14\text{-}C19 \rightarrow \pi^*C24\text{-}C26$		89.83
$\pi C16\text{-}C21 \rightarrow \pi^*C13\text{-}C18$	82.01	84.14
$\pi C16\text{-}C21 \rightarrow \pi^*C23\text{-}C25$	87.65	88.74
$\pi C17\text{-}C22 \rightarrow \pi^*C14\text{-}C19$		81.93
$\pi C17\text{-}C22 \rightarrow \pi^*C24\text{-}C26$		86.86
$\pi C19\text{-}C24 \rightarrow \pi^*C14\text{-}C17$	81.38	
$\pi C19\text{-}C24 \rightarrow \pi^*C22\text{-}C26$	89.62	
$\pi C20\text{-}C27 \rightarrow \pi^*N11\text{-}C15$	119.34	117.54
$\pi C20\text{-}C27 \rightarrow \pi^*C28\text{-}C29$	71.94	70.85
$\pi C22\text{-}C26 \rightarrow \pi^*C14\text{-}C17$	82.93	
$\pi C22\text{-}C26 \rightarrow \pi^*C19\text{-}C24$	79.42	
$\pi C23\text{-}C25 \rightarrow \pi^*C13\text{-}C18$	81.30	80.13
$\pi C23\text{-}C25 \rightarrow \pi^*C13\text{-}C18$	81.55	83.26
$\pi C24\text{-}C26 \rightarrow \pi^*C14\text{-}C19$		80.05
$\pi C24\text{-}C26 \rightarrow \pi^*C17\text{-}C22$		84.43
$\pi C28\text{-}C29 \rightarrow \pi^*N11\text{-}C15$	68.55	67.46
$\pi C28\text{-}C29 \rightarrow \pi^*C20\text{-}C27$	95.01	95.09
$\boldsymbol{\Delta ET_{\pi \rightarrow \pi^*}}$	**1532.92**	**1538.93**
$LP(2)O5 \rightarrow \sigma^*S1\text{-}O7$	59.52	62.28
$LP(2)O5 \rightarrow \sigma^*S1\text{-}O8$	57.93	57.43
$LP(3)O5 \rightarrow \sigma^*S1\text{-}O3$	116.16	102.66
$LP(2)O6 \rightarrow \sigma^*S2\text{-}O9$	59.60	60.53
$LP(2)O6 \rightarrow \sigma^*S2\text{-}O10$	57.85	59.23
$LP(3)O6 \rightarrow \sigma^*S2\text{-}O4$	115.70	102.24
$LP(2)O7 \rightarrow \sigma^*S1\text{-}O5$	70.81	64.58
$LP(2)O7 \rightarrow \sigma^*S1\text{-}O8$	76.16	75.20
$LP(3)O7 \rightarrow \sigma^*S1\text{-}O3$	185.13	153.40
$LP(2)O8 \rightarrow \sigma^*S1\text{-}O5$	71.94	64.62
$LP(2)O8 \rightarrow \sigma^*S1\text{-}O7$	76.66	75.78

(*Continued*)

http://dx.doi.org/10.1016/j.heliyon.2016.e00190

Table 4. (*Continued*)

Delocalization	Gas	PCM
*LP(3)O8 → σ*S1-O3*	188.60	155.83
*LP(2)O9 → σ*S2-O6*	70.51	64.41
*LP(2)O9 → σ*S2-O10*	76.03	75.32
*LP(3)O9 → σ*S2-O4*	183.96	153.65
*LP(2)O10 → σ*S2-O6*	72.06	64.66
*LP(2)O10 → σ*S2-O9*	76.87	75.57
*LP(3)O10 → σ*S2-O4*	188.64	154.87
*LP(1)N11 → σ*C15-C20*		42.26
$\Delta ET_{LP\rightarrow\sigma^*}$	**1804.13**	**1664.52**
*σS1-O3→ π*C23-C25*	61.15	
*σS2-O4→ π*C22-C26*	69.97	
$\Delta ET_{\sigma\rightarrow\pi^*}$	**131.12**	
*σS1-O5→ σ*S1-O7*	71.23	92.25
*σS1-O5→ σ*S1-O8*	70.85	93.04
*σS2-O6→ σ*S2-O9*	71.60	92.59
*σS2-O6→ σ*S2-O10*	70.39	92.33
$\Delta ET_{\sigma\rightarrow\sigma^*}$	**284.07**	**370.21**
*π*N11-C15→π*C20-C27*	1075.84	1116.56
*π*N11-C15→π*C28-C29*	884.44	748.55
*π*C23-C25→π*S1-O3*		158.13
*π*C23-C25→π*C13-C18*	1107.11	
*π*C24-C26→π*S2-O4*		184.21
*π*C24-C26→π*C14-C19*		1078.31
$\Delta ET_{\pi^*\rightarrow\pi^*}$	**3067.39**	**3285.76**
ΔE_{Total}	**6819.63**	**6859.42**

Na43···O5, Na44···O4, Na44···O6) and the other ones are H bond interactions (O7···H36, N11···H33, N11···H34 and O9···H37) with very low $\rho(r)$ and $\nabla^2\rho(r)$ values. In solution, the number of H bond interactions is notably reduced from 4 to 1 and, where in some cases, the $\rho(r)$ and $\nabla^2\rho(r)$ values increase (S···O) while in other ones decrease (Na···O, N−H), as observed in Table 5. These analyses clearly support: (i) the high stabilities of APS in both media, (ii) the ionic nature of APS and, (iii) the different characteristics of the S−O bonds belonging to the SO_4^{2-} groups and of Na−O bonds present in sodium picosulfate.

http://dx.doi.org/10.1016/j.heliyon.2016.e00190

Table 5. Analysis of the topological properties for sodium picosulfate in both media by using the B3LYP/6-31G* method.

Parameter (a.u.)	**S1···O3**	**S1···O5**	**S1···O7**	**S1···O8**	**Na43···O3**	**Na43···O5**	**O7···H36**	**N11···H33**	**N11···H34**	**S2···O4**	**S2···O6**	**S2···O9**	**S2···O10**	**Na44···O4**	**Na44···O6**	**O9···H37**
$\rho(r_c)$	0.1544	0.2682	0.2865	0.2872	0.0267	0.0317	0.0069	0.0140	0.0084	0.1549	0.2683	0.2863	0.2874	0.0268	0.0314	0.0076
$\nabla^2\rho(r_c)$	−0.0910	0.6997	1.0500	1.0644	0.1920	0.2235	0.0273	0.0462	0.0304	−0.0940	0.6999	1.0466	1.0669	0.1882	0.2204	0.0292
λ_1	−0.2328	−0.4491	−0.4872	−0.4884	−0.0348	−0.0438	−0.0047	−0.0137	−0.0062	−0.2330	−0.4493	−0.4869	−0.4887	−0.0351	−0.0432	−0.0063
λ_2	−0.2211	−0.4199	−0.4395	−0.4398	−0.0325	−0.0406	−0.0012	−0.0122	−0.0016	−0.2215	−0.4206	−0.4399	−0.4403	−0.0328	−0.0400	−0.0036
λ_3	0.3629	1.5688	1.9768	1.9927	0.2544	0.3079	0.0333	0.0721	0.0382	0.3605	1.5698	1.9734	1.9960	0.2561	0.3037	0.0391
$\lvert\lambda_1\rvert/\lambda_3$	0.6415	0.2863	0.2465	0.2451	0.1368	0.1423	0.1411	0.1900	0.1623	0.6463	0.2862	0.2467	0.2448	0.1371	0.1422	0.1611
Distance (Å)	1.810	1.500	1.461	1.460	2.191	2.151	2.743	2.376	2.742	1.807	1.500	1.461	1.459	2.190	2.156	2.665
Parameter (a.u.)	S1···O3	S1−O5	S1−O7	S1−O8	Na43···O3	Na43···O5		N11···H33		S2···O4	S2−O6	S2−O9	S2−O10	Na44···O4	Na44···O6	
$\rho(r_c)$	0.1800	0.2716	0.2833	0.2835	0.0201	0.0247		0.0088		0.1804	0.2715	0.2833	0.2835	0.0202	0.0247	
$\nabla^2\rho(r_c)$	−0.2020	0.7773	0.9332	0.9353	0.1252	0.1551		0.0302		−0.2033	0.7852	0.9340	−0.9330	0.1262	0.1554	
λ_1	−0.2623	−0.4560	−0.4741	−0.4744	−0.0236	−0.0312		−0.0073		−0.2630	−0.4560	−0.4743	−0.4741	−0.0237	−0.0312	
λ_2	−0.2476	−0.4409	−0.4367	−0.4353	−0.0227	−0.0290		−0.0031		−0.2481	−0.4412	−0.4363	−0.4355	−0.0228	−0.0290	
λ_3	0.3081	1.6743	1.8440	1.8451	0.1715	0.2154		0.0410		0.3079	1.6757	1.8446	1.8427	0.1728	0.2157	
$\lvert\lambda_1\rvert/\lambda_3$	0.8513	0.2724	0.2571	0.2571	0.1376	0.1448		0.1780		0.8542	0.2721	0.2571	0.2573	0.1372	0.1446	
Distance (Å)	1.720	1.493	1.472	1.472	2.316	2.263		2.617		1.719	1.493	1.472	1.472	2.313	2.263	

http://dx.doi.org/10.1016/j.heliyon.2016.e00190

3.4. Frontier orbital and quantum molecular descriptors studies

Since long time it is highly known that the gap values can predict the reactivity of a drug in different media by using the frontier orbitals [27, 28]. On the other hand, their behaviours in different media can also be predicted by using diverse descriptors such as, the chemical potential (μ), electronegativity (χ), global hardness (η), global softness (S), global electrophilicity index (ω) and global nucleophilicity index (E) descriptors [29, 30, 31, 32, 33]. In this work, we have calculated for APS in both media the gap values and those descriptors at B3LYP/6-31G* level of theory. These parameters in both media can be seen in Table 6 together with the corresponding equations and compared with those observed for drugs with potential antimicrobial activity, as the 1,3-benzothiazole tautomers [33] and with antiviral properties as cidofovir and brincidofovir [38]. These compounds have different rings and groups, as can be observed in Fig. 5. Analyzing the gap values, we observed that the thione form of 1,3-benzothiazole is the most reactive than the other ones while the reactivity decrease according to the following order: thione > brincidofovir > sodium picosulfate > thiol > cidofovir. When the descriptors are deeply analyzed, we observed that the most reactive thione present

Table 6. Calculated HOMO and LUMO orbitals, energy band gap, chemical potential (μ), electronegativity (χ), global hardness (η), global softness (S) and global electrophilicity index (ω) for sodium picosulfate in gas phase and in aqueous solution.

B3LYP/6-31G* method[a]								
Frontier orbitals (eV)	**Sodium picosulfate**		**thione[b]**		**thiol[b]**		**Cidofovir[c]**	**brincidofovir[c]**
	Gas	**PCM**	**Gas**	**PCM**	**Gas**	**PCM**	**Gas**	**Gas**
HOMO	−5.912	−6.100	−6.4443	−6.4066	−6.8847	−6.9012	−5.9366	−5.5435
LUMO	−1.949	−2.173	−2.7918	−2.8545	−2.6194	−2.6679	−0.6401	−1.772
GAP	−3.963	−3.927	−3.6525	−3.5521	−4.2653	−4.2333	−5.2965	−3.7715
Descriptors (eV)								
χ	−1.9815	−1.9635	−1.8263	−1.7761	−2.1327	−2.1167	−2.6483	−1.8858
μ	−3.9305	−4.1365	−4.61805	−4.63055	−4.7521	−4.7846	−3.2884	−3.6578
η	1.9815	1.9635	1.8263	1.7761	2.1327	2.1167	2.6483	1.8858
S	0.2523	0.2546	0.2738	0.2815	0.2345	0.2362	0.1888	0.2651
ω	3.8983	4.3572	5.8388	6.0364	5.2943	5.4076	2.0416	3.5474
E;	−7.7883	−8.1220	−8.4337	−8.2241	−10.1345	−10.1272	−8.7087	−6.8979

$S = ½\eta; \omega = \mu^2/2\eta$; $E = \mu^*\eta$.

$\chi = -[E(LUMO) - E(HOMO)]/2$; $\mu = [E(LUMO) + E(HOMO)]/2$; $\eta = [E(LUMO) - E(HOMO)]/2$;.

[a] This work.

[b] From [33],[c]From [38].

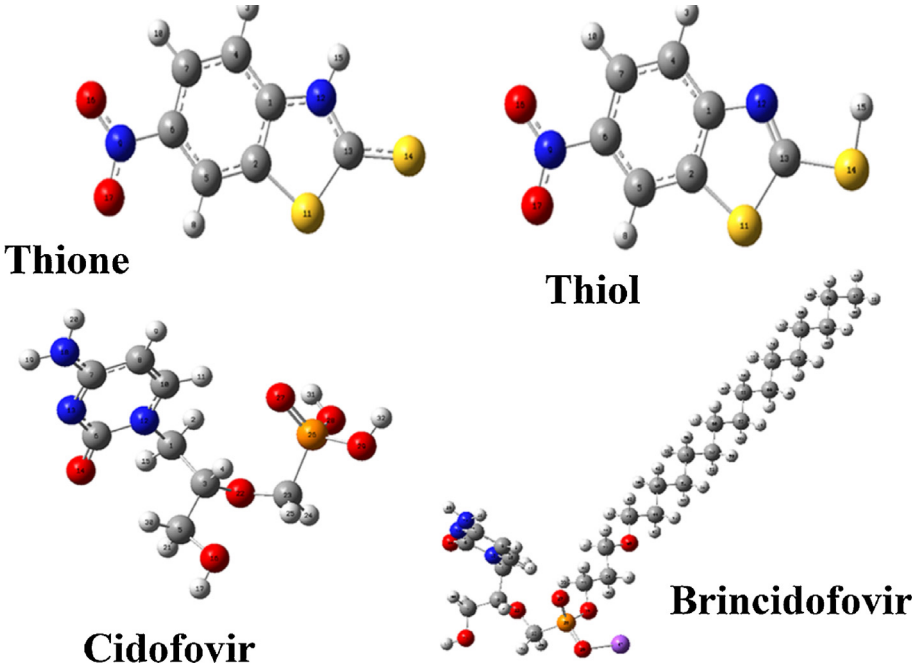

Fig. 5. Structures of the different compounds compared with anhydrous sodium picosulfate in gas phase.

the higher electrophilicity index while cidofovir has the most low index. Apparently both parameters are related to the presence of strong charged groups, as the NO_2^- and S−H groups that in the thiol form due to the presence of an H bond decreases their reactivity, as compared with the thione form. Brincidofovir has slightly higher reactivity than picosulfate and much higher than cidofovir due to the presence of a PO_4^{3-} group and of a Na atom, here, evidently the presence of a group with higher charge increase the reactividad in brincidofovir. Probably, a high nucleophilicity index together with a high electrophilicity index reduce the reactivity of a drug, as observed for cidofovir because the separation between both indexes is of approximately 4–3 eV while in the most reactive thione that separation is about 3–2 eV. Sodium picosulfate presents reactivity similar to brincidofovir probably due to the presence of two SO_4^{2-} groups and of the two Na atoms in their structure. The other parameters such as, global hardness (η) and softness (S) are in very good concordance with the order of reactivity, as expected because both descriptors are calculated directly from the gap values.

3.5. NMR study

The ^{1}H- and ^{13}C-NMR chemical shifts for APS in gas phase and in aqueous solution phases were calculated by using the GIAO method [34] at the B3LYP/6-31G* level of theory and the results are presented in Table 7 and Table 8, respectively. Here, the ^{1}H- NMR chemical shifts were compared with the

http://dx.doi.org/10.1016/j.heliyon.2016.e00190

Table 7. Observed in DMSO-d_6 and calculated ^{1}H chemical shifts (δ in ppm) for sodium picosulfate in gas phase and aqueous solution.

H atom	Sodium picosulfate[a]		Pred.[c]	Exp[b]
	Gas	PCM		
30-H	5.15	5.55	5.51	2.50
31-H	7.38	7.43	7.51	7.08
32-H	7.40	7.27	7.51	7.20
33-H	8.63	7.68	7.51	8.52
34-H	8.32	7.56	7.51	7.74
35-H	7.43	7.34	7.27	7.22
36-H	7.58	7.63	7.08	7.24
37-H	7.69	7.46	7.08	7.70
38-H	7.19	7.31	7.08	5.57
39-H	7.14	7.49	7.08	3.34
40-H	7.74	7.68	7.69	7.72
41-H	9.11	9.02	8.53	8.53
42-H	7.28	7.22	7.21	7.05
RMSD	**1.39**	**1.54**	**1.44**	

[a] This work GIAO/B3LYP/6-31G* Ref. to TMS.

[b] From [39].

[c] From [40].

corresponding experimental available for APS in DMSO-d6 from [39] and with the predicted by Spinus-Web [40] by means of the RMSD values. The comparison of the calculated ^{13}C-NMR chemical shifts was performed with those ^{13}C-NMR predicted by Banfi and Patiny [41] and Castillo et al. [42] by means of the RMSD values, as observed in Table 7. Notice that a better correlation is observed for the H nuclei (1.54–1.39 ppm) than the C nuclei (9.14–8.73 ppm), as expected because the calculations were performed using the B3LYP/6-31G* calculations in gas phase and in aqueous solution while the experimental ^{1}H-NMR spectrum was registered in DMSO-d6 solution. In aqueous solution, the presences of the SO_4^{2-} groups and of Na atoms evidently have certain influence on the chemical shifts of both nuclei because APS has a higher affinity in water than DMSO.

3.6. Vibrational study

The structures of APS in the two media using the B3LYP/6-31G* level of theory were optimized with C_1 symmetries and both structures have 126 normal vibration modes which present activity in both IR and Raman spectra. The available experimental IR spectrum for the monohydrated sodium picosulphate in the solid phase was taken from [43] and can be seen in Fig. 6 compared with the predicted

http://dx.doi.org/10.1016/j.heliyon.2016.e00190

Table 8. Calculated ^{13}C chemical shifts (δ in ppm) for sodium picosulfate in gas phase and in aqueous solution.

C atoms	Sodium picosulfate[a]		Pred.[b]
	Gas	PCM	
12-C	71.06	71.33	40.95
13-C	144.70	144.35	141.23
14-C	143.99	144.06	141.23
15-C	167.12	168.38	162.39
16-C	134.27	134.69	126.66
17-C	133.04	133.64	126.66
18-C	131.64	134.19	126.66
19-C	134.88	135.96	126.66
20-C	127.53	127.24	118.43
21-C	127.54	128.19	121.75
22-C	126.30	127.48	121.75
23-C	127.23	127.93	121.75
24-C	127.05	128.47	121.75
25-C	154.03	153.24	151.67
26-C	154.77	153.15	151.67
27-C	138.95	138.53	136.80
28-C	153.28	154.58	149.33
29-C	124.73	124.23	123.37
RMSD	**8.73**	**9.14**	

[a] This work GIAO/B3LYP/6-31G* Ref. to TMS.

[b] From [41, 42].

by the calculations in gas phase and in aqueous solution at the same level of theory. The vibrational assignments for APS in both media were performed with the SQMFF procedure [17, 18] by using the Molvib program [19] and taking into account the PED contributions ≥ 10%. The symmetry coordinates used in the determination of the force fields were similar to those reported for compounds containing analogous rings and groups [2, 3, 4, 30, 31] for this reason, they were not presented here. On the other hand, the scale factors used are those reported by Rauhut and Pulay and defined for the 6-31G* basis set [17, 18]. Table 9 shows the observed and calculated wavenumbers and assignments for anhydrous sodium picosulfate in both media. Obviously, we observed higher quantity of bands in the experimental spectrum due to the vibration modes of the water molecule, hence, the broad IR bands at 3639 and 3458 cm^{-1} are clearly attributed to the OH stretching modes. Note that the very intense band predicted by the calculations in gas phase at 606 cm^{-1} and assigned easily to the symmetric $\delta_s SO_3$ deformation

http://dx.doi.org/10.1016/j.heliyon.2016.e00190

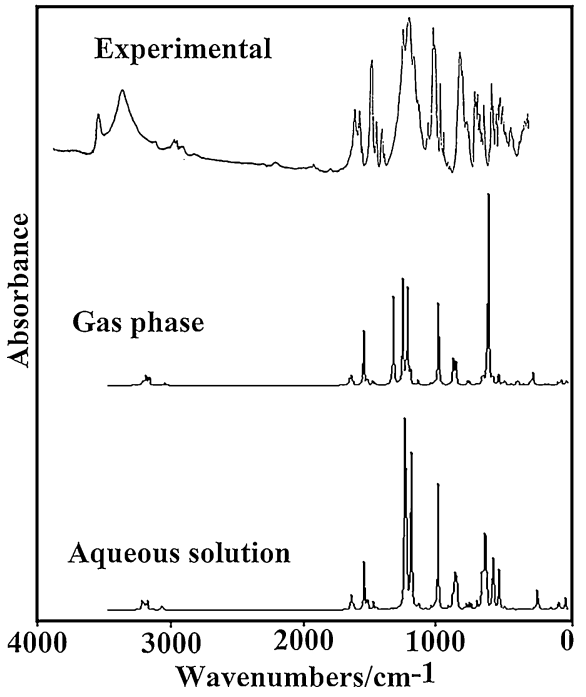

Fig. 6. Experimental available infrared spectra of sodium picosulfate hydrate (upper) taken from [43] and the corresponding anhydrous predicted in gas phase (medium) and in aqueous solution (bottom) by using B3LYP/6-31G* level of theory.

mode in solution decrease significantly their intensity probably due to that the $\Delta E_{n\rightarrow\sigma^*}$ charges transfers related to the O atoms of these groups decrease from 1804,13 kJ/mol in gas phase to 1664,52 kJ/mol in solution, as observed in Table 4. This variation can also be attributed to the topological properties of the S−O bonds because in solution two of these bonds are enlarged while the other two shortened, as observed by AIM calculations (Table 5). The predicted Raman spectra for APS in both media by using the same method of calculation are compared in Fig. 7. We present below a brief discussion of the assignments for some groups.

3.7. Band Assignments

3.7.1. SO_4^{2-} groups

Normally, the asymmetric and symmetric stretching and bending modes of these groups for a tetrahedral structure are expected between 1150 and 320 cm^{-1} [1, 44, 45, 46] while in potassium borosulfate, where three sulphate groups have C_{3v} symmetries, the antisymmetric and symmetric modes were assigned to the bands at 1375 and 884 cm^{-1}. Here, the broad and intense band between 1342 and 1146 cm^{-1}, centred at 1258 cm^{-1}, obviously is assigned to the four antisymmetric stretching modes expected for both SO_4^{2-} groups while the corresponding symmetric modes are assigned to the intense IR band at 892 cm^{-1}, as indicated in

http://dx.doi.org/10.1016/j.heliyon.2016.e00190

Table 9. Observed and calculated wavenumbers (cm^{-1}) and assignments for anhydrous sodium picosulfate in both media.

Experimental[c]	B3LYP/6-31G* Method[a]			
IR	Gas phase		Aqueous solution	
solid	SQM[b]	Assignments	SQM[b]	Assignments
3639w				νOH H_2O
3458m				νOH H_2O
3100 sh	3103	νC19-H34	3100	νC18-H33
	3096	νC21-H36	3097	νC21-H36
	3091	νC18-H33	3096	νC29-H42
	3084	νC29-H42	3095	νC24-H39
	3072	νC20-H35	3086	νC23-H38
	3069	νC22-H37	3085	νC20-H35
3068w	3068	νC24-H39	3083	νC19-H34
	3068	νC23-H38	3074	νC27-H40
	3058	νC27-H40	3072	νC17-H32
3047w	3049	νC16-H31	3070	νC16-H31
	3045	νC17-H32	3059	νC22-H37
2999w	3041	νC28-H41	3057	νC28-H41
2915w	2932	νC12-H30	2950	νC12-H30
1653m	1606	νC16-C21	1600	νC16-C21,νC23-C18
1616m	1593	νC27-C20	1592	νC28-C29,νC20-C15
1600 sh	1586	νC24-C19,νC14-C17	1583	νC18-C13,νC13-C16
1560 sh	1579	νC18-C13,νC13-C16	1580	νC14-C17,νC26-C24
1541 sh	1577	νC29-C27	1571	νC29-C27,νC15-N11
1529s	1560	νC19-C14,νC26-C24	1562	νC19-C14,νC22-C26
1495m	1502	βC16-H31	1498	βC16-H31,νC21-C25
1462m	1479	βC24-H39	1476	βC28-H41,βC20-H35
1454m	1476	βC28-H41,βC20-H35	1471	βC24-H39
1438w	1436	βC29-H42	1429	βC29-H42
	1420	νC23-C18	1416	ρC12-H30
	1405	ρ'C12-H30,βC17-H32,βC19-H34	1396	βC17-H32
1347 sh	1355	βC28-H41	1345	ρ'C12-H30
	1324	ρC12-H30	1327	ρ'C12-H30,ρC12-H30
1301s	1306	βC22-H37	1302	βC19-H34
1271 sh	1295	νC25-C23,νC21-C25	1298	νC25-C23
	1284	νC22-C26	1281	νN11-C28
1258 vs	1274	$\nu_a SO_3(2)$	1266	νN11-C28
	1272	$\nu_a SO_3(1)$	1246	νC19-C14,ρC12-H30

(*Continued*)

http://dx.doi.org/10.1016/j.heliyon.2016.e00190

Table 9. (*Continued*)

Experimental[c]	B3LYP/6-31G* Method[a]			
IR	**Gas phase**		**Aqueous solution**	
solid	**SQM[b]**	**Assignments**	**SQM[b]**	**Assignments**
	1271	νN11-C28	1240	νC15-N11
1226s	1239	νC15-N11	1192	νC25-O3
	1234	ρC12-H30,νC19-C14	1190	$\nu_a SO_3(1)$
1196sh	1211	νC25-O3	1190	$\nu_a SO_3(2)$
1183 sh	1204	νC26-O4	1185	νC26-O4
	1186	νC20-C15 νC12-C15	1184	νC12-C15
	1177	$\nu_a SO_3(1)$	1176	νC12-C13
	1175	$\nu_a SO_3(2)$	1159	βC21-H36
1166 sh	1166	νC12-C13	1158	βC22-H37
	1163	βC23-H38	1152	νC12-C14,νC24-C19
1130 sh	1161	$\nu_a SO_3(2)$,νC26-O4	1143	$\nu_a SO_3(2)$
1121w	1157	νC12-C14	1143	βC27-H40
	1151	βC27-H40	1142	$\nu_a SO_3(1)$
	1105	βC21-H36,βC18-H33	1101	βC23-H38
1086s	1092	βC29-H42,νC17-C22	1089	νC17-C22
1073 sh	1090	νC17-C22	1088	νC27-C20
1033m	1044	νC28-C29	1043	νC29-C27
1009w	1020	$\beta R_1(1)$	1016	$\beta R_1(1)$
	996	$\beta R_1(3)$	1012	γC27-H40
	995	γC27-H40	994	$\beta R_1(3)$
	993	$\beta R_1(2)$	992	$\beta R_1(2)$
979w	975	γC18-H33	980	γC28-H41
965w	966	γC28-H41	972	γC18-H33
952w	949	γC16-H31	963	γC19-H34
892s	948	$\nu_s SO_3(2)$	959	γC16-H31
892s	947	$\nu_s SO_3(1)$	951	$\nu_s SO_3(1)$
	942	γC24-H39	950	$\nu_s SO_3(2)$
	933	γC17-H32	947	γC17-H32
	900	γC20-H35	911	γC20-H35
871m	889	γC22-H37	888	γC24-H39
	868	γC23-H38	875	γC23-H38
842m	854	δC13C12C15	856	δC13C12C15
826 sh	837	γC19-H34	836	γC23-H38,γC24-H39
	830	νC26-O4	831	γC23-H38

(*Continued*)

http://dx.doi.org/10.1016/j.heliyon.2016.e00190

Table 9. (*Continued*)

Experimental[c]	B3LYP/6-31G* Method[a]			
IR	Gas phase		Aqueous solution	
solid	SQM[b]	Assignments	SQM[b]	Assignments
	828	γC21-H36	829	γC21-H36
	824	γC19-H34	822	γC24-H39
	811	γC22-H37	816	γC22-H37
783m	809	δC13C12C14	806	δC13C12C14
762m	763	γC29-H42	769	γC29-H42
747w	747	$tR_1(3)$	752	$tR_1(3)$
731w	730	$tR_1(2)$	729	$tR_1(2)$
718w	710	$tR_1(1)$	711	$tR_1(1)$
676 sh	686	$\beta R_2(3),\beta R_3(3)$	681	$\beta R_2(3)$
660m	646	$\beta R_2(1),\beta R_3(1)$	644	$\beta R_3(1)$
650w	640	$\beta R_2(3)$	642	$\beta R_2(1)$
630 sh	629	$\beta R_2(2)$	631	$\beta R_2(2)$
625w	620	$\beta R_3(3)$	626	νS1-O3
610w	610	$\beta R_3(2)$	621	$\beta R_3(2)$
598m	600	$\delta_s SO_3(2)$	615	νS2-O4
581w	596	$\delta_s SO_3(1)$	608	$\beta R_3(3)$
575 sh	565	$tR_1(1)$	565	$\delta_s SO_3(1)$
560 sh	564	$tR_1(2)$	563	$\delta_s SO_3(2)$
528 sh	525	$\delta_a SO_3(1)$	523	$\delta_a SO_3(1)$
	524	$\delta_a SO_3(2)$	522	$\delta_a SO_3(2)$
521w	519	$\delta_a SO_3(1)$	518	$\delta_a SO_3(2)$,γC26-O4
514 sh	514	$\delta_a SO_3(2)$,γC26-O4	514	$\delta_a SO_3(1)$,γC25-O3,γC13-C12
500 sh	490	$tR_2(3)$,γC15-C12	498	$tR_2(3)$
	477	$tR_2(2)$	473	$tR_2(2)$
458 sh	468	$tR_2(1)$	468	$tR_2(1)$
429 sh	437	βC25-O3	441	βC25-O3
421w	422	βC26-O4	435	βC26-O4
	412	$tR_3(1)$	415	$tR_3(1)$
405w	405	$tR_3(3)$	408	$tR_3(2)$
398w	399	$tR_3(2)$	407	$tR_3(3)$
	380	νO6-Na44	373	νS1-O3
	366	$\rho SO_3(1)$	355	νS2-O4,$tR_1(2)$
	333	νS2-O4	342	$\rho SO_3(1)$
	313	νS1-O3	322	$\rho SO_3(2)$
	303	$\rho'sO_3(1)$	310	$\rho'sO_3(1)$

(*Continued*)

http://dx.doi.org/10.1016/j.heliyon.2016.e00190

Table 9. (*Continued*)

Experimental[c]	B3LYP/6-31G* Method[a]			
IR	Gas phase		Aqueous solution	
solid	SQM[b]	Assignments	SQM[b]	Assignments
	294	ρ'sO$_3$(2)	298	ρ'sO$_3$(2)
	280	νO5-Na43	257	βC15-C12
	268	ρSO$_3$(2)	248	νO5-Na43,δS1O5Na43
	264	δS1O5Na43	230	νO5-Na43
	244	βC15-C12	226	νO6-Na44
	234	ρ'sO$_3$(2),βC15-C12	215	βC14-C12
	206	βC13-C12,βC14-C12	206	βC13-C12
	179	tR$_2$(1),tR$_2$(2)	181	tR$_2$(2),tR$_2$(1)
	169	tR$_2$(2),νO5-Na43	155	δC25O3S1
	145	tR$_2$(2),ρSO$_3$(2)	131	δS1O5Na43
	134	δC25O3S1	120	δS2O6Na44
	92	δC13C12C15	86	δC26O4S2
	72	γC25-O3	71	δC26O4S2
	67	δC26O4S2,δC14C12C15	67	τ$_w$C25-O3
	50	τNa44-O6	60	τNa43-O5
	49	τNa43-O5	59	τNa44-O6
	47	τNa43-O5,τ$_w$C15-C12	57	τ$_w$C14-C12
	39	twSO$_3$(2)	51	τ$_w$C15-C12
	37	twSO$_3$(1)	47	τ$_w$C25-O3,τ$_w$C13-C12
	32	τ$_w$C13-C12	35	twSO$_3$(2)
	26	τ$_w$C15-C12	29	γC14-C12
	21	τ$_w$C14-C12	27	τ$_w$C13-C12
	13	τ$_w$C26-O4	19	twSO$_3$(1)
	11	γC14-C12	18	τ$_w$C13-C12,τ$_w$C14-C12
	4	τ$_w$C25-O3	15	τ$_w$C26-O4

Abbreviations: ν, stretching; β, deformation in the plane; γ, deformation out of plane; wag, wagging; τ, torsion; β$_R$, deformation ring τ$_R$, torsion ring; ρ, rocking; τw, twisting; δ, deformation; a, antisymmetric; s, symmetric; ($_1$), glucopyranose Ring1; ($_2$), glucopyranose Ring2.

[a] This work.

[b] From scaled quantum mechanics force field.

[c] From [43].

Table 9. Notice that in solution these stretching modes are shifted toward lower wavenumbers, as expected because these modes are strongly affected by the hydration, as was previously analyzed. Here, the symmetric bending modes are predicted by calculations at higher wavenumbers (600–596 cm^{-1}) than the corresponding antisymmetric modes (525–514 cm^{-1}) and; for this reason, they

http://dx.doi.org/10.1016/j.heliyon.2016.e00190

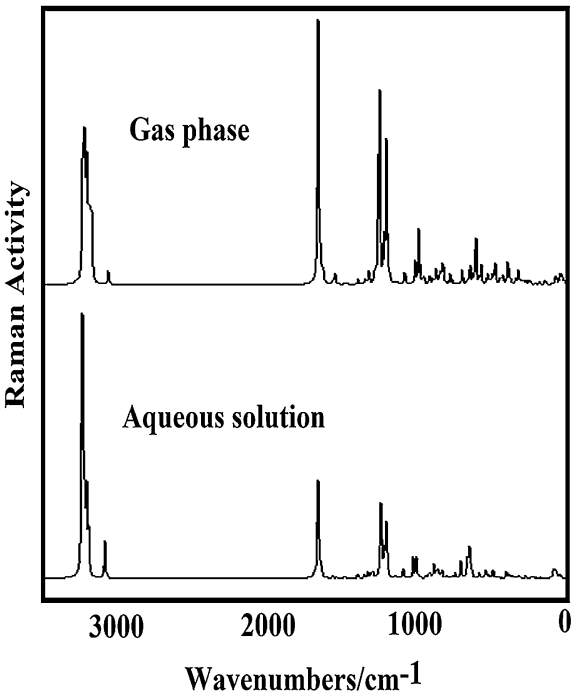

Fig. 7. Predicted Raman spectra of anhydrous sodium picosulfate in gas phase and in aqueous solution at B3LYP/6-31G* level of theory.

were assigned to the band and shoulder at 598 and 591 cm^{-1}, respectively. In solution, all these modes are predicted between 565 and 514 cm^{-1} because are influenced by the hydration. The four rocking and the two twisting modes expected for both sulphate groups are clearly predicted in gas phase in the 303–268 and 39–37 cm^{-1} regions, respectively and, both modes were not assigned because in the IR spectrum were recorded bands only up to 398 cm^{-1}. This vibrational analysis shows clearly the influence of the different S−O bonds of the sulphate groups on the positions of the IR bands and, in particular, in aqueous solution support the shifting of the bands related to these groups as a consequence of the hydration.

3.7.2. Pyridinyl and phenyl rings modes.

The thirteen expected C−H stretching modes are predicted in gas phase between 3103 and 2932 cm^{-1} where the C12−H30 bond related to the C atom with hybridization sp^3, is predicted to lower wavenumbers than the other ones. Thus, the bands observed between 3100 and 2915 cm^{-1} are clearly assigned to those vibration modes. In solution, these modes are predicted slightly to higher wavenumbers, as observed in Table 9 probably due to that these H atoms are involved in gas phase to two N···H and two O···H bonds while in solution only the N···H is observed. The in-plane C−H deformation modes are assigned to the bands

http://dx.doi.org/10.1016/j.heliyon.2016.e00190

observed between 1495 and 1086 cm^{-1} because they are predicted by SQM calculations in this region while the corresponding out-of-plane CH deformation modes are assigned according to calculation between 1009 and 762 cm^{-1}. These modes are not affected by the hydration because they undergo few shifted in solution. The C=C stretching modes of both phenyl rings are predicted by the SQM/B3LYP/6-31G* calculations between 1606 and 1560 cm^{-1} while the C−C stretching modes between 1420 and 1044 cm^{-1}, hence these modes are assigned according to calculations. On the other hand, the two expected C−N stretching modes belonging to the pyridinyl ring are predicted at 1271 and 1239 cm^{-1} while in solution are predicted to higher wavenumbers. This observation can be attributed to the two N···H bonds observed only in gas phase while in solution only one of them is observed. Moreover, two transitions observed by NBO calculation justify the shifting observed in solution, they are the $\Delta ET_{\pi\rightarrow\pi^*}$ and $\Delta ET_{\pi\rightarrow\pi^*}$ charge transfers (see Table 4). The deformation and torsion modes for both pyridinyl and phenyl rings are predicted by SQM calculations in the expected regions [4, 28, 29, 30, 31, 32] and only some deformation modes were assigned because the torsion modes are predicted in the lower wavenumbers region where there are not observed bands. The assignments for the remaining skeletal modes can be seen in Table 9.

3.8. Force fields

The force constants for APS in both media were first calculated in Cartesian coordinates from their corresponding force fields by using the SQM procedure and later they were transformed to internal coordinates with the Molvib program [17, 18, 19]. These constants are summarized in Table 10 compared with those reported for $CrO_2(SO_3F)_2$ [3] and benzisoxazole methane sulfonic acid sodium salt (BOSNa) [4] and, with those calculated in this work for $K_5[B(SO_4)_4]$. Analyzing first the force constants values for APS in both media we observed that practically the $f(\nu C\text{-}C)_{A6}$, $f(\nu C\text{-}C)$ and $f(\nu C\text{-}H)$ constants change slightly in solution, especially the latter increase because the H bonds decrease in this media, as suggested by the above studies. The other constants change notably due to the structural changes that experiment the both SO_4^{2-} groups and the Na···O bonds in solution. When the constants for APS are compared with those observed for $CrO_2(SO_3F)_2$ [3] the values are higher in this chromyl compound because their three S=O bonds have double bound character while the high value observed in the $f(\nu S\text{-}F)$ constant is due to the presence of the F atom instead of other O atom. On the other hand, the $f(\nu S{=}O)$ constant is higher in APS than that calculated for BOSNa because only three S=O bonds have this species while that a higher value is observed in their $f(\nu C{-}N)$ constant due to that the N atoms are linked to C and O atoms instead of two C atoms, as in APS and, besides these bonds belong to a five member ring instead of a six member ring, as in APS. However, the $f(\nu Na{-}O)$ constant values

http://dx.doi.org/10.1016/j.heliyon.2016.e00190

Table 10. Comparison of scaled internal force constants for sodium picosulfate in both media with those calculated for compounds with similar groups.

Force constant	B3LYP/6-31G*[a]				B3P86/6-31G*[a]	
	Picosulfate		$CrO_2(SO_3F)_2$[b]	BOSNa[c]	$K_5[B(SO_4)_4]$	
	Gas	PCM	Gas	Gas	Force constant	Gas
f(νS═O)	8.25	7.79	10.6	7.27	*f(νS═O)*	8.7
f(νS-X)	1.65	2.37	4.7		*f(νS-O)*	4.3
$f(\nu C\text{-}C)_{A6}$	6.50	6.51		6.48		
f(νC-N)	7.03	6.87		8.17		
f(νC-C)	3.97	4.00				
(νC-O)	5.33	5.01		5.72		
f(νNa-O)	0.88	0.52		0.82	*f(νK-O)*	1.42
f(νC-H)	5.18	5.21				
f(δO═S═O)	1.72	1.59	1.6	1.91	*f(δO═S═O)*	2.0
f(δS-O-C)	0.87	0.95				
f(δC-C-C)	1.83	1.93				
f(δS-O-Na)	2.56	1.33			*f(δS-O-B)*	0.40

Units are mdyn $Å^{-1}$ for stretching and mdyn Å rad^{-2} for angle deformations, A6, pyridinyl and phenyl Rings.

[a] This work.

[b] From [3].

[c] From [4] for benzisoxazole methane sulfonic acid sodium salt (BOSNa); X = (O,F).

are practically similar in these compounds while in $K_5[B(SO_4)_4]$ the presence of the most electropositive K atom increase notably the constant value in this borate compound. Moreover, the presence of five sulphate groups evidently increase the values of the *f(νS═O) f(νS−O)* and *f(δO═S═O)* constants, as compared with that observed in APS. Obviously, this study also support the differences in the S═O, S−O and Na···O bonds and their modifications in solution.

3.9. Electronic spectrum

The electronic spectrum for APS in aqueous solution was predicted by B3LYP/6-31G* calculations and their comparison with the experimental available UV-visible spectrum reported for the sodium picosulphate hydrate [47] can be seen in Fig. 8. A strong band at 262.54 nm is observed in the experimental spectrum while in the predicted spectrum is calculated at 234.50 nm which can be easily assigned to the $\pi \rightarrow \pi^*$ and $\pi^* \rightarrow \pi^*$ interactions due to the C═C and C−N bonds because the calculations predicted these interaction with higher energy values, as observed by

http://dx.doi.org/10.1016/j.heliyon.2016.e00190

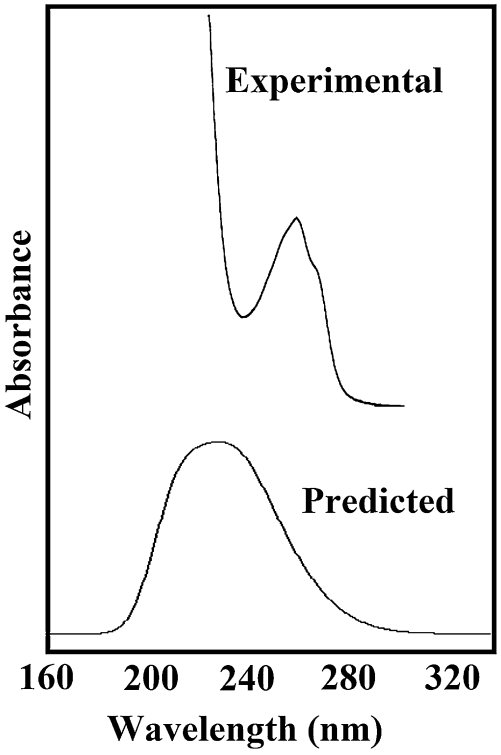

Fig. 8. Comparisons between the experimental available UV-Vis spectrum of sodium picosulfate hydrate (upper) taken from [47] and the theoretical spectrum of the anhydrous form (bottom) by using B3LYP/6-31G* level of theory.

NBO analysis (Table 4). Here, the presence of shoulders in the experimental spectrum could be attributed to the quantity observed of these interactions as a consequence of the three six member's rings in the structure of APS. Table 11 shows the positions and intensities of the observed bands in the experimental spectrum and in the predicted by the TD-DFT calculations.

Table 11. TD-DFT calculated visible absorption wavelengths (nm) and oscillator strengths (f) for sodium picosulfate in aqueous solution.

B3LYP6-31G*,[a]			Experimental[b]	
Energy Transition[a] (eV)	λ(nm)	f	λ(nm)	Assignment[a]
5.9557	208.18	0.1042	157.00 sh	π→π* (C=C)
5.2871	234.50	0.1413	262.54 s	π→π* (C-N)
5.1603	240.26	0.1700	268.80 sh	π*→π*(C=C)

[a] This work.

http://dx.doi.org/10.1016/j.heliyon.2016.e00190

4. Conclusions

In this work, the theoretical molecular structures of anhydrous sodium picosulfate with chemical formula $C_{18}H_{13}NNa_2O_8S_2$, was optimized in gas and aqueous solution phases by using the B3LYP/6-31G* method. The influences of the solvent on their properties were studied with the IFEPCM and SM models. The AIM results show clearly the presence of the S═O, S−O, Na···O, N···H and O···H bonds with different characteristics, thus, in each sulphate group is observed one covalent S−O bond where the O atoms are linked to the C atoms, three highly polar covalent S═O bonds and two ionic Na−O bonds. Besides, in gas phase are predicted two N···H and O···H bonds while in solution disappear one N···H bond and the two O···H bonds. The nature of those bonds belonging to the two C-O-SO_3-O-Na groups and, evidenced by AIM calculations, have notable influence on the NPA and MK charges, MEP values, reactivities, descriptors, vibration normal modes and force constants in both media. On the other hand, the high stabilities of sodium picosulfate are supported by the NBO in both media and evidenced by the strong band observed in the electronic spectrum in solution. Here, the force fields using the B3LYP/6-31G* method and the complete assignments of the 126 vibration normal modes expected for sodium picosulfate in both media are presented. The predicted infrared, ^{1}H-NMR and UV-visible spectra are in reasonable concordance with the corresponding available experimental spectra. In addition, the frontier orbitals show the high reactivities of sodium picosulfate in both media which is approximately comparable to brincidofovir, an antiviral drug used against the *Ebola* disease.

Declarations

Author contribution statement

Davide Romani: Analyzed and interpreted the data; Contributed reagents, materials, analysis tools or data.

Isabel Salas Tonello: Performed the experiments.

Silvia A. Brandán: Conceived and designed the experiments; Performed the experiments; Analyzed and interpreted the data; Contributed reagents, materials, analysis tools or data; Wrote the paper.

Funding statement

This work was supported by CIUNT (Consejo de Investigaciones, Universidad Nacional de Tucumán).

http://dx.doi.org/10.1016/j.heliyon.2016.e00190

Competing interest statement

The authors declare no conflict of interest.

Additional information

No additional information is available for this paper.

References

[1] A. Periasamy, S. Murugan, M. Palaniswamy, Vibrational studies of Na_2SO_4, K_2SO_4, $NaHSO_4$ and $KHSO_4$ crystals, Rasayan J. Chem. 2 (4) (2009) 981.

[2] H.A. Höppe, K. Kazmierczak, E. Romano, S.A. Brandán, A structural and vibrational study on the first potassium borosulfate, $K_5[B(SO_4)_4]$ by using the FTIR-Raman and DFT calculations, J. Mol. Struct. 1037 (2013) 294–300.

[3] S.A. Brandán, Volume 1: A Structural and Vibrational Study of the Chromyl Chlorosulfate, Fluorosulfate, and Nitrate Compounds, In: Ken Derham (Ed.), Springer Science, Business Media B.V., Van Godewijckstraat 30 3311 GZ Dordrecht, Netherlands, 2012 978-94-007-5762-2 (Print) 978-94-007-5763-9 (Online).

[4] M.J. Márquez, M.B. Márquez, S.A. Brandán, Chapter 6: A structural and spectroscopic study on benzisozaxole methane sulfonic acid sodium salt (BOSNa), In: A. Silvia Brandán (Ed.), Descriptors, Structural and spectroscopic Properties of Heterocyclic derivatives of importance for the health and the enviromental, Edited Collection, Nova Science Publishers Inc., 2015, 2016978-1-63482-708-9, pp. 132–157.

[5] J. Love, E.J. Bernard, A. Cockeram, L. Cohen, M. Fishman, J. Gray, D. Morgan, A multicentre, observational study of sodium picosulfate and magnesium citrate as a precolonoscopy bowel preparation, Can. J. Gastroenterol. 23 (10) (2009) 706–710.

[6] L.J. Scott, A.J. Wagstaff, Sodium picosulfate/magnesium citrate: a review of its use as a colorectal cleanser, Drugs 69 (1) (2009) 123–136.

[7] H.-P. Tee, C. Corte, H. Al-Ghamdi, E. Prakoso, J. Darke, R. Chettiar, W. Rahman, S. Davison, S.P. Griffin, W.S. Selby, A.J. Kaffes, Prospective randomized controlled trial evaluating cap-assisted colonoscopy vs standard colonoscopy, World J. Gastroenterol. 16 (31) (2010) 3905–3910.

[8] A.R. Liu, A.X. Garg, K. Liu, S.Z. Shariff, A.K. Jain, M.A. Weir, Increased Risk of Adverse Renal Outcome Following Polyethylene Glycol Bowel Preparation Compared to Sodium Picosulfate, J. Clin. Pharmacol. 56 (8) (2016) 983–987.

 http://dx.doi.org/10.1016/j.heliyon.2016.e00190

[9] K. Kathiresan, M. Kathiravan, P. Pandian, S.P. Nayak, R. Manavalan, Analytical method development and validation of pendo-purgative by RP-HPLC, Rasayan J. Chem. 2 (2) (2009) 293–296.

[10] I. Savić, G. Nikolić, I. Savić, Quantitative analysis of sodium picosulfate in the presence of its alkaline degradation product, Macedonian J. Chem. Chem. Eng. 28 (2) (2009) 151–158.

[11] A.D. Becke, Density functional thermochemistry. III. The role of exact exchange, J. Chem. Phys. 98 (1993) 5648–5652.

[12] C. Lee, W. Yang, R.G. Parr, Development of the Colle-Salvetti correlation-energy formula into a functional of the electron density, Phys. Rev. B 37 (1988) 785–789.

[13] A.E. Reed, L.A. Curtis, F. Weinhold, Intermolecular interactions from a natural bond orbital, donor-acceptor viewpoint, Chem. Rev. 88 (6) (1988) 899–926.

[14] E.D. Glendening, J.K. Badenhoop, A.D. Reed, J.E. Carpenter, F. Weinhold, NBO 3.1 Theoretical Chemistry Institute, University of Wisconsin, Madison, WI, 1996.

[15] R.F.W. Bader, Atoms in Molecules A Quantum Theory, Oxford University Press, Oxford, 19900198558651, pp. 458.

[16] F. Biegler-Köning, J. Schönbohm, D.J. Bayles, AIM2000 - A program to analyze and visualize atoms in molecules, J. Comput. Chem. 22 (2001) 545–559.

[17] G. Rauhut, P. Pulay, Transferable scaling factors for density functional derived vibrational force fields, J. Phys. Chem. 99 (1995) 3093–3099.

[18] G. Rauhut, P. Pulay, Erratum - Transferable scaling factors for density functional derived vibrational force fields, J. Phys. Chem. 99 (1995) 14572.

[19] T. Sundius, Scaling of ab-initio force fields by MOLVIB, Vib. Spectrosc. 29 (2002) 89–95.

[20] A.B. Nielsen, A.J. Holder, Gauss View Usefs Reference, GAUSSIAN, Inc., Pittsburgh, P.A., USA, 2000-2003.

[21] M.J. Frisch, G.W. Trucks, H.B. Schlegel, G.E. Scuseria, M.A. Robb, J.R. Cheeseman, G. Scalmani, V. Barone, B. Mennucci, G.A. Petersson, H. Nakatsuji, M. Caricato, X. Li, H.P. Hratchian, A.F. Izmaylov, J. Bloino, G. Zheng, J.L. Sonnenberg, M. Hada, M. Ehara, K. Toyota, R. Fukuda, J. Hasegawa, M. Ishida, T. Nakajima, Y. Honda, O. Kitao, H. Nakai, T. Vreven, J.A. Montgomery Jr., J.E. Peralta, F. Ogliaro, M. Bearpark, J.J. Heyd, E.

 http://dx.doi.org/10.1016/j.heliyon.2016.e00190

Brothers, K.N. Kudin, V.N. Staroverov, R. Kobayashi, J. Normand, K. Raghavachari, A. Rendell, J.C. Burant, S.S. Iyengar, J. Tomasi, M. Cossi, N. Rega, J.M. Millam, M. Klene, J.E. Knox, J.B. Cross, V. Bakken, C. Adamo, J. Jaramillo, R. Gomperts, R.E. Stratmann, O. Yazyev, A.J. Austin, R. Cammi, C. Pomelli, J.W. Ochterski, R.L. Martin, K. Morokuma, V.G. Zakrzewski, G. A. Voth, P. Salvador, J.J. Dannenberg, S. Dapprich, A.D. Daniels, Ö. Farkas, J.B. Foresman, J.V. Ortiz, J. Cioslowski, D.J. Fox, Gaussian 09 Revision D.01, Gaussian Inc., Wallingford CT, 2009.

[22] J. Tomasi, J. Persico, Molecular Interactions in Solution: An Overview of Methods Based on Continous Distributions of the Solvent, Chem. Rev. 94 (1994) 2027–2094.

[23] S. Miertus, E. Scrocco, J. Tomasi, Electrostatic interaction of a solute with a continuum, Chem. Phys. 55 (1981) 117–129.

[24] P. Ugliengo, MOLDRAW Program, University of Torino, Dipartimento Chimica IFM, Torino, Italy, 1998.

[25] A.V. Marenich, C.J. Cramer, D.G. Truhlar, Universal solvation model based on solute electron density and a continuum model of the solvent defined by the bulk dielectric constant and atomic surface tensions, J. Phys. Chem. 113 (2009) 6378–6396.

[26] B.H. Besler, K.M. Merz Jr., P.A. Kollman, Atomic charges derived from demiempirical methods, J. Comp. Chem. 11 (1990) 431–439.

[27] R.G. Parr, R.G. Pearson, Absolute hardness: companion parameter to absolute electronegativity, J. Am. Chem. Soc. 105 (1983) 7512–7516.

[28] J.-L. Brédas, Mind the gap!, Mater. Horiz. 1 (2014) 17–19.

[29] P.G. Cataldo, M.V. Castillo, S.A. Brandán, Quantum mechanical modeling of fluoromethylated-pyrrol derivatives. A study on their reactivities, structures and vibrational properties, J. Phys. Chem. Biophys. 4 (1) (2014) 2–9.

[30] M.B. Márquez, S.A. Brandán, A structural and vibrational investigation on the antiviral deoxyribonucleoside thymidine agent in gas and aqueous solution phases, Int. J. Quantum Chem. 114 (3) (2014) 209–221.

[31] M.J. Márquez, M.B. Márquez, P.G. Cataldo, S.A. Brandán, A comparative study on the structural and vibrational properties of two cyanopyridine derivatives with potentials antimicrobial and anticancer activities, OJSTA 4 (2015) 1–19.

 http://dx.doi.org/10.1016/j.heliyon.2016.e00190

[32] D. Romani, S.A. Brandán, M.J. Márquez, M.B. Márquez, Structural, topological and vibrational properties of an isothiazole derivatives series with antiviral activities, J. Mol. Struct. 1100 (2015) 279–289.

[33] D. Romani, S.A. Brandán, Structural electronic and vibrational studies of two 1,3-benzothiazole tautomers with potential antimicrobial activity in aqueous and organic solvents. Prediction of their reactivities, Comp. Theor. Chem. 1061 (2015) 89–99.

[34] R. Ditchfield, Self-consistent perturbation theory of diamagnetism. I. A gage-invariant LCAO (linear combination of atomic orbitals) method for NMR chemical shifts, Mol. Phys. 27 (1974) 789–807.

[35] Q. Sun, T. Xiao, P. Chen, X. Gan, L. Bao, Bis[μ-1,2-diphenyl-NN'-bis-(di-2-pyridyl-methyl-eneamino)ethane-1, 2-diimine]disilver(I) bis-(hexa-fluorido-phosphate) acetonitrile disolvate, Acta Cryst. B70 (2014) 714–722.

[36] E.M.S. Leduc, R.C. Peterson, R. Wang, Sodium magnesium sulfate deca-hydrate, $Na_2Mg(SO_4)_2.10H_2O$, a new sulfate salt, Acta Cryst. C65 (2009) i81–i84.

[37] I.S. Bushmarinov, K.A. Lyssenko, M. Yu Antipin, Atomic energy in the Atoms in Molecules theory and its use for solving chemical problems, Russian Chem. Rev. 78 (4) (2009) 283–302.

[38] D. Romani, S.A. Brandán, Effect of the side chain on the properties from cidofovir to brincidofovir, an experimental antiviral drug against to Ebola virus disease, Arabian Journal of Chemistry (2015).

[39] Selleck Chem, Sodium Picosulfate, (2016) . NMR-DMSO-d6 http://www.selleckchem.com/products/sodium-picosulfate.html.

[40] Spinus Web, Prediction of full proton NMR spectra, (2016) . http://www2.chemie.uni-erlangen.de/services/spinus/.

[41] D. Banfi, L. Patiny, Resurrecting and processing NMR spectra on-line, Chimia 62 (4) (2008) 280–281 www.nmrdb.org.

[42] A.M. Castillo, L. Patiny, J. Wist, Fast and Accurate Algorithm for the Simulation of NMR spectra of Large Spin Systems, J. Magn. Reson. 209 (2) (2011) 123–130.

[43] Infrared Reference Spectra, Sodium Picosulfate Hydrate, (2016) , pp. 1496. www.pmda.go.jp/files/000152623.pdf.

[44] J.T. Kloprogge, R.D. Schuiling, Z. Ding, L. Hickey, H. Ruan, D. Wharton, R. L. Frost, Vibrational spectroscopic study of syngenite formed during the treatment of liquid manure with sulphuric acid, Vibrat. Spect. 28 (2002) 209.

 http://dx.doi.org/10.1016/j.heliyon.2016.e00190

[45] P. Dawson, M.M. Hargrjzave, G.R. Wilkinson, Polarized IR reflection, absorption and laser Raman studies on a single crystal of $BaSO_4$, Spetrochim. Acta 33A (1977) 83.

[46] E. Knittle, W. Phillips, Q. Williams, A infrared and Raman spectroscopic study of gypsum at high pressures, Phys. Chem. Minerals 28 (2001) 630.

[47] Ultraviolet-visible Reference Spectra, (2016) , pp. 2114. www.pmda.go.jp/files/000152525.pdf.

 http://dx.doi.org/10.1016/j.heliyon.2016.e00190